



# Nanocrystalline thin films synthesized from a Ti<sub>2</sub>AlN compound target by high power impulse magnetron sputtering technique

Teng Fei Zhang<sup>a,b</sup>, Qi Min Wang<sup>b,c,\*</sup>, Junghoon Lee<sup>a</sup>, Peiling Ke<sup>d</sup>, Roman Nowak<sup>e</sup>, Kwang Ho Kim<sup>a,b,\*\*</sup>

<sup>a</sup> School of Materials Science and Engineering, Pusan National University, Busan 609-735, South Korea

<sup>b</sup> National Core Research Center for Hybrid Materials Solution, Pusan National University, Busan 609-735, South Korea

<sup>c</sup> School of Electromechanical Engineering, Guangdong University of Technology, Guangzhou 510006, China

<sup>d</sup> Division of Surface Engineering, Ningbo Institute of Materials Technology and Engineering, Chinese Academy of Sciences, Ningbo 315201, China

<sup>e</sup> Nordic Hysitron Laboratory, Department of Materials Science & Engineering, Aalto University, 00076 Aalto, Finland

## ARTICLE INFO

### Article history:

Received 20 May 2012

Accepted in revised form 27 September 2012

Available online 5 October 2012

### Keywords:

MAX-phase films

High power impulse magnetron sputtering

(HIPIMS)

High resolution TEM (HRTEM)

Mechanical properties

Oxidation

Corrosion

## ABSTRACT

Ti–Al–N thin films were synthesized utilizing a high power impulse magnetron sputtering (HIPIMS) from a Ti<sub>2</sub>AlN compound target. The deposition temperatures and bias voltages were varied in the range of room temperature (RT) to 450 °C and 0 V to –70 V, respectively. It was indicated that amorphous films formed at low deposition temperatures of RT and 300 °C, which changed into MAX-phase Ti<sub>2</sub>AlN films after vacuum annealing at 800 °C for 1 h. Densely packed nano-fibrous crystalline films mainly composing of Ti<sub>2</sub>AlN MAX phase and tetragonal Ti<sub>2</sub>N phase were acquired at deposition temperature of 450 °C, which exhibited stable film structure during vacuum annealing at 800 °C. The Ti<sub>2</sub>AlN–Ti<sub>2</sub>N composite films exhibited excellent oxidation and corrosion resistance, as compared to (Ti,Al)N film having same Ti/Al ratio and/or TiN film synthesized by a hybrid coating system with HIPIMS and DC pulse magnetron sputtering. The mechanical properties of the Ti<sub>2</sub>AlN–Ti<sub>2</sub>N films were also investigated in this work.

© 2012 Elsevier B.V. All rights reserved.

## 1. Introduction

The M<sub>n+1</sub>AX<sub>n</sub> (abbreviated as MAX, where M is an early transition metal, A is an IIIA- or IVA-group element, X is C or N, and n = 1, 2, or 3) phases are a family of nanolaminated compounds with M<sub>n+1</sub>X<sub>n</sub> layers being interleaved with layers of A-atoms [1–3]. Due to their unique structure and interesting combinations of metallic and ceramic behavior, MAX phases have been fabricated both in bulk materials and in film types. MAX phases belong to high-order material systems. A significant amount of thermally activated atom diffusion is required to form these large-unit-cell phases. The MAX-phase films generally form at high deposition temperature, which is limiting the application of MAX-phase films.

High power impulse magnetron sputtering (HIPIMS) is a novel physical vapor deposition (PVD) technique. By pulsing the sputtering target with high power (e.g. 1–3 kW/cm<sup>2</sup>), short duration (<200 μs) pulses, a high ionization of the sputtered species can be obtained, without significant target heating. HIPIMS has been shown to have several

merits over conventional sputtering, such as increased film density and good adhesion; as well as some advantages over vacuum arc deposition, e.g., free from macroparticles and smooth surface. Especially, due to increased high ionization, the adatom mobility and reactivity at low temperatures can be much improved [4–9], which makes HIPIMS have great potential to synthesize the high-order materials at a low deposition temperature. Alami et al. [10] considered utilizing HIPIMS technique to grow MAX-phase films. They deposited Ti–Si–C films using HIPIMS from a Ti<sub>3</sub>SiC<sub>2</sub> compound target and observed the presence of the Ti<sub>5</sub>Si<sub>3</sub>C<sub>x</sub> phase. However, due to the complexity of growing higher-order material systems, despite the possibility of synthesizing MAX-phase films using HIPIMS techniques at low temperature, no MAX-phase Ti<sub>3</sub>SiC<sub>2</sub> was obtained in Alami's work [10]. The use of HIPIMS technique to grow high-order material systems, for instance ternary MAX phases, is far from being well investigated.

In a set of researches of MAX-phase materials, Ti<sub>2</sub>AlN is far from being well explored. Some efforts had been made with respect to the fabrication of Ti<sub>2</sub>AlN MAX-phase films. Ti<sub>2</sub>AlN single crystalline films were epitaxially grown on single-crystalline MgO and Al<sub>2</sub>O<sub>3</sub> substrates by reactive magnetron sputtering Ti, Al and Ti<sub>2</sub>Al targets in a mixed Ar–N<sub>2</sub> atmosphere [2,3,11–13]. Two-step deposition-annealing processes were also adopted to synthesize Ti<sub>2</sub>AlN MAX-phase films [14,15]. During thermal annealing after deposition, solid state reaction occurred, which resulted in the formation of

\* Correspondence to: Q.M. Wang, National Core Research Center for Hybrid Materials Solution, Pusan National University, Busan 609-735, South Korea.

\*\* Correspondence to: K.H. Kim, National Core Research Center for Hybrid Materials Solution, Pusan National University, Busan 609-735, South Korea. Tel.: +82 51 510 2391; fax: +82 51 510 3660.

E-mail addresses: [qmwang@gdut.edu.cn](mailto:qmwang@gdut.edu.cn) (Q.M. Wang), [kwhokim@pusan.ac.kr](mailto:kwhokim@pusan.ac.kr) (K.H. Kim).

Ti<sub>2</sub>AlN phases [16–18]. In all of these studies, main problems still remain to be solved, such as high synthesis temperature (over 690 °C). For the industrial application, in-situ formation of MAX-phase Ti<sub>2</sub>AlN films at low deposition temperature is needed.

In this study, we try to utilize HIPIMS technique to synthesize Ti<sub>2</sub>AlN films. Given the fact that deposition of higher-order-material systems often requires sputtering from several sources, it is highly beneficial that deposition of Ti–Al–N films can be carried out from a single Ti<sub>2</sub>AlN target. Therefore, we fabricated the films by magnetron sputtering a Ti<sub>2</sub>AlN compound target in an Ar atmosphere. The deposition temperatures and bias voltages were varied to change the adatom mobility during film deposition. After film deposition, the thermal annealing behavior, mechanical properties, oxidation and corrosion performance of the films were investigated.

## 2. Experimental details

### 2.1. Sample preparation

A coating system with a modulated pulse power (HIPIMS + power, Hauzer Techno Coating BV) applying on the sputtering cathode was utilized for deposition. Table 1 summarizes the HIPIMS pulsing parameters. A fully dense polycrystalline Ti<sub>2</sub>AlN compound target with a diameter of 80 mm and a thickness of 1 cm, which was fabricated by a spark plasma sintering (SPS) method, was utilized. EPMA analysis showed that the target had an atomic composition of Ti:Al:N:O = 0.47:0.22:0.25:0.06. XRD results indicated that the Ti<sub>2</sub>AlN target was composed of pure Ti<sub>2</sub>AlN MAX phase. The films were deposited on the ultrasonic cleaned (100)-orientated single crystalline Si wafers and (0006)-orientated single crystalline Al<sub>2</sub>O<sub>3</sub> wafers in a vacuum chamber with a base pressure less than  $4 \times 10^{-3}$  Pa. The substrate temperature was controlled at room temperature (RT), 300 °C or 450 °C, respectively. The chamber pressure was kept at 0.5 Pa by injecting the Ar gas near the target. An average power of 0.8 kW, peak current density of 0.98 A/cm<sup>2</sup>, repetition rate of 36 (Hz) was applied on the target cathode by the modulated pulse power. A bias voltage of 0 to –70 V was supplied on the substrate which was facing the sputtering target with a target-substrate distance of about 8 cm. The deposition rate and time were 0.9–1.2 μm/h and 4–8 h, respectively. The film thickness was controlled by adjusting the deposition time.

To conduct comparison experiment in the oxidation and corrosion test in this study, (Ti,Al)N and TiN films were also synthesized using a hybrid coating system with HIPIMS and DC pulse magnetron sputtering. (Ti,Al)N film was fabricated by co-sputtering using Ti (modulated pulse power) and Al (pulse DC power) dual-targets in an Ar + N<sub>2</sub> atmosphere at a temperature of 300 °C. By adjusting the sputtering power of Ti and Al target, (Ti,Al)N film having same Ti/Al ratio with the Ti<sub>2</sub>AlN–Ti<sub>2</sub>N film was obtained. TiN film was synthesized by a reactive magnetron sputtering using Ti target (modulated pulse power) in an Ar + N<sub>2</sub> atmosphere at a temperature of 300 °C.

### 2.2. Film characterization

Elementary compositions of the deposited films were investigated by electron probe micro-analysis (EPMA, Shimadzu, EPMA-1600. Ti: CAMECA Company, 100% Ti standard; Al: CAMECA Company, 100%

**Table 1**  
The HIPIMS pulsing parameters for Ti–Al–N films deposition.

Pulsing parameters	P <sub>a</sub> [kW]	P <sub>p</sub> [kW]	I <sub>a</sub> [A]	I <sub>p</sub> [A]	V <sub>a</sub> [V]	V <sub>p</sub> [V]	I <sub>d</sub> [A/cm <sup>2</sup> ]
36 Hz and 5.1% duty cycle	0.8	37.1	23.1	49.0	678.6	756.4	0.98

P<sub>a</sub> and P<sub>p</sub> are the average and peak target power.

I<sub>a</sub> and I<sub>p</sub> are the average and peak target current in one pulse length.

V<sub>a</sub> and V<sub>p</sub> are the average and peak target voltage.

I<sub>d</sub> is the peak target current density during the pulse.

Al standard; N: CAMECA Company, 56.44% N in BN standard; O: P & H Development Ltd. Company, 40.05% O in TiO<sub>2</sub> standard). X-ray diffraction (XRD, D8-Discovery Brucker, Cu Kα, 40 kV, 40 mA) and 2-dimensional X-ray diffraction (2D-XRD, D8-Discover with GADDS Brucker, Cu Kα, 3 kW) were used to characterize the phase and crystallinity of the deposited films. Samples for transmission electron microscopy (TEM) analysis were prepared by a focused ion beam (FIB) technique. Relevant cross-sectional TEM analysis was conducted in a field emission JEOL-2010F analytical electron microscope operated at 200 kV.

### 2.3. Film performance

The micro-hardness of the films was investigated using a nano-indentation tester (MTS NANO G200). The residual stress of the coatings was obtained from a laser-based curvature measurement of the coated Si-substrates by calculating using the Stoney's equation [19].

Isothermal oxidation tests were conducted in static air atmosphere in a muffle furnace by heating the Al<sub>2</sub>O<sub>3</sub> specimens coated with Ti<sub>2</sub>AlN–Ti<sub>2</sub>N films and (Ti,Al)N films at 900 °C for 1–5 h. The oxidation products on the oxidized specimens were characterized by XRD analysis. The scanning electron microscopy (SEM, Hitachi, S-4800, 15 kV) equipped with an energy dispersive X-ray spectrometer (EDX) were used to investigate the oxide scale formed on the films after oxidation.

The potentiodynamic polarization curves for the Si specimens without and with deposited films were obtained to investigate the corrosion performance of the films utilizing a potentiostat (Versastat 4) in a 3.5 wt.% sodium chloride (NaCl) solution at room temperature. A silver/silver chloride and platinum (Pt) mesh were used as a reference electrode and a counter electrode, respectively. For comparison, not only the electrochemical corrosion behavior of the Ti<sub>2</sub>AlN–Ti<sub>2</sub>N film, but also that of the (Ti,Al)N film having same Ti/Al ratio with the Ti<sub>2</sub>AlN–Ti<sub>2</sub>N film and TiN films were investigated by a potentiodynamic polarization test. The surface and cross sections of the specimens after corrosion tests were observed by SEM.

## 3. Results and discussion

### 3.1. Film characterization

#### 3.1.1. Compositional analysis

Table 2 shows the chemical compositions of the Ti<sub>2</sub>AlN target and the Ti–Al–N films as determined by EPMA. It can be seen that the chemical compositions of the films deposited at a substrate temperature of RT, 300 °C and 450 °C deviated from that of the target. Al was excessive in the film deposited at RT and was deficient in the films deposited at 300 °C and 450 °C, while N was deficient in the films deposited at RT, 300 °C and 450 °C, as compared to the target composition.

Reasons for excessive Al in the film deposited at RT: for the Al atoms with smaller diameter, it may suffer less collisions and gas-phase scattering during transport from target to substrate than Ti atoms due to its longer mean free path (the mean free path of Al atoms in argon gas is 1.3 times higher than that of Ti atoms at the same Ar gas pressure [20]). Reasons for Al deficiency in the films deposited at 300 °C and 450 °C: as the deposition temperature increases, the evaporation of the Al element became the main factor

**Table 2**

The EPMA results of the Ti<sub>2</sub>AlN target and the Ti–Al–N films deposited at RT, 300 °C and 450 °C, respectively.

	Ti (at.%)	Al (at.%)	N (at.%)	O (at.%)
Target	47.0	22.4	24.5	6.01
Deposition temperature (°C)	RT	52.3	28.2	13.3
	300	53.6	25.9	14.1
	450	54.8	24.4	14.4

influencing the film composition. As for the MAX phases, evaporative loss of the A element during thin-film growth has been observed in several MAX phase studies. Frodelius et al. [21] reported Al deficiency during deposition of  $Ti_2AlC$  MAX phase from a  $Ti_2AlC$  compound target. Deficiency of other A-elements has been reported in the Ti–Si–C, V–Ge–C, and Cr–Al–C systems [22–26]. In this study, the strong temperature dependence of the Al content is not surprising considering the high vapor pressure of metallic Al. In addition, the depositions were conducted at relatively low temperatures. Therefore, the Al deficiency was not so important as compared to other studies.

The N deficiency in the films deposited at RT, 300 °C and 450 °C can be explained by the different effusion rate of atom species influenced by their molecular mass. Target elements in plasma mostly exist as neutral atomic gas phase. According to the Graham's law, the rate of effusion of a gas is inversely proportional to the square root of its molecular mass. This formula can be written as:

$$\frac{Rate_1}{Rate_2} = \sqrt{\frac{M_2}{M_1}}$$

where  $Rate_1$  and  $Rate_2$  are the rates of effusion of the first gas and the second gas, respectively;  $M_1$  and  $M_2$  are the molar masses of gas 1 and gas 2, respectively. It was considered that N atoms diffused faster than Ti and Al atoms to the zone close to pump region (lower gas pressure) due to their smaller molecular mass and were pumped out of chamber by the vacuum system. This effect may result in a lower concentration of N in the gas phase plasma than that in the compound target.

### 3.1.2. Phase structure

Fig. 1 shows the XRD patterns of Ti–Al–N films deposited on Si(100) wafers at RT, 300 °C, and 450 °C. As shown in Fig. 1(a), the films deposited below 450 °C were all amorphous films. At deposition temperature of 450 °C, one strong single diffraction peak appeared at 62.5°. Variation of bias voltage at the deposition temperature of 450 °C in the range of 0 to –70 V resulted in no significant change in the phase structure of the films except a little shifting of the diffraction peak (Fig. 1(b)). The peak shifting should be related to the residual stress in the films. To characterize the peak at 62.5°, we compared the three possibilities:  $Ti_2AlN$  (110) plane (62.2°), TiN (220) plane (61.8°), or  $Ti_2N$  (220) plane (63.3°). The peak is closest to the  $Ti_2AlN$  (110) plane. By considering the fact that the content of N + O

in the films less than 21 at.%, we can exclude the possibility of TiN existence.

The films obtained in this study are highly preferred orientation. To obtain the phase structure information of the films other than the planes parallel to the specimen surface, we conducted 2D-XRD by tilting the Chi angles at 30°, 45°, 60°, and 90°, respectively. Fig. 2 shows the 2D-XRD diffraction patterns of the films deposited on  $Al_2O_3$  at 450 °C and bias voltage of –60 V. Both diffraction peaks attributed to the  $Ti_2AlN$  MAX-phase and  $Ti_2N$  phases can be observed at Chi tilting angles of 30°, 45°, 60° and 90°. Figs. 1 and 2 indicated that the Ti–Al–N films deposited at 450 °C were composed of  $Ti_2AlN$  MAX phase and tetragonal  $Ti_2N$  phase. We named these films as  $Ti_2AlN$ – $Ti_2N$  films.

Fig. 3 shows the cross-sectional TEM images of the  $Ti_2AlN$ – $Ti_2N$  film deposited at 450 °C and bias voltage of –60 V. The film was composed of densely packed nanocrystalline fibrous grains [Fig. 3(a) and (b)]. Very fine crystallites with diameter less than 10 nm were observed. The selected area diffraction pattern (SADP) in Fig. 3(c) showed a pattern of diffraction spots instead of a ring pattern. Even with increasing selected area aperture up to 2.5  $\mu m$  in size, which is the whole film thickness, only spot patterns were observed. This means that the film is strongly textured, with only several planes existing in the direction of cross-section. The largest devotion to the strongly textured microstructure came from the  $Ti_2AlN$  (110) planes. Other planes such as  $Ti_2AlN$  (101),  $Ti_2N$  (004), and  $Ti_2N$  (312) were also observed. Fig. 3(d) and (e) shows the high-resolution TEM (HRTEM) images of the  $Ti_2AlN$ – $Ti_2N$  film. From the lattice fringes and the corresponding Fast Fourier Transformation (FFT) patterns, well-crystallized  $Ti_2AlN$  and  $Ti_2N$  grains were observed. As shown in Fig. 3(d), the d values of lattice fringes and the corresponding FFT pattern were perfectly consistent with (110) plane of the  $Ti_2AlN$  MAX-phase. In Fig. 3(e), the lattice fringes and the FFT patterns can be attributed to (200) and (220) planes of the  $Ti_2N$  phase. These results are consistent with the 2D-XRD analyses of Fig. 2. The films are composed of  $Ti_2AlN$  and  $Ti_2N$  phases. The strong (110) preferred orientation of  $Ti_2AlN$  grains in this study instead of (001) texture in other report [2] seems to be related to highly strained condition of HIPIMS process, but needs further investigation. The  $Ti_2N$  phase should come into being by Al deficiency in the  $Ti_2AlN$  phase, which will be further discussed later.

Fig. 4 shows the XRD patterns of the Ti–Al–N films after vacuum annealing at 800 °C for 1 h. It can be seen that the Ti–Al–N films deposited at RT and 300 °C transformed from amorphous to pure  $Ti_2AlN$  MAX-phase. These results indicated that the composition of the Ti–Al–N films was proper enough to form MAX-phase  $Ti_2AlN$ . The film deposited at 450 °C, which was composed of  $Ti_2AlN$  and  $Ti_2N$  phases, didn't change phase structure during post annealing

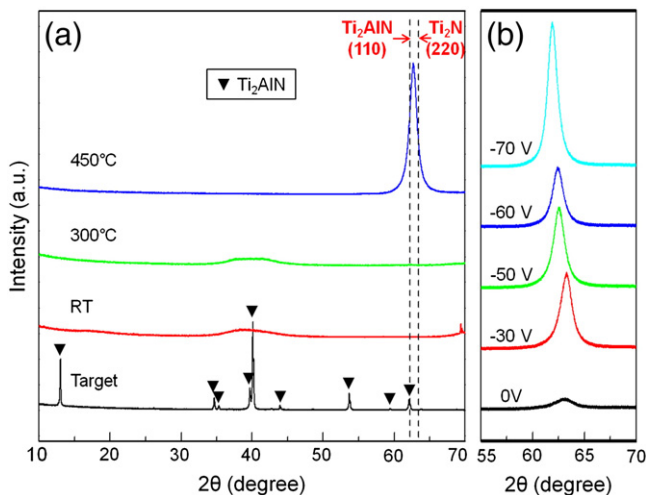


Fig. 1. XRD patterns of (a) Ti–Al–N films deposited at RT, 300 °C and 450 °C and bias voltage of –50 V (b) Ti–Al–N films deposited at 450 °C and bias voltage of 0 V, –30 V, –50 V, –60 V and –70 V, respectively.

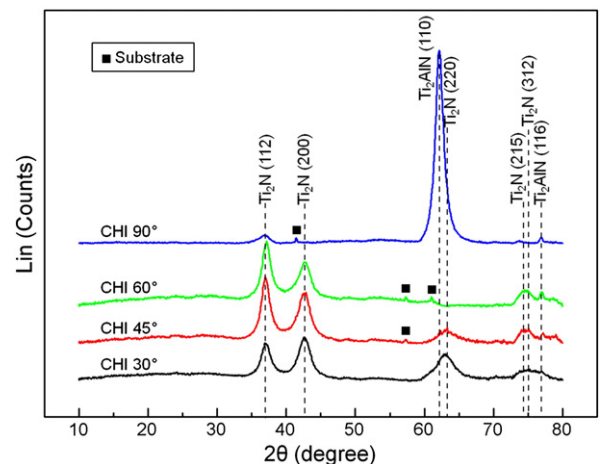
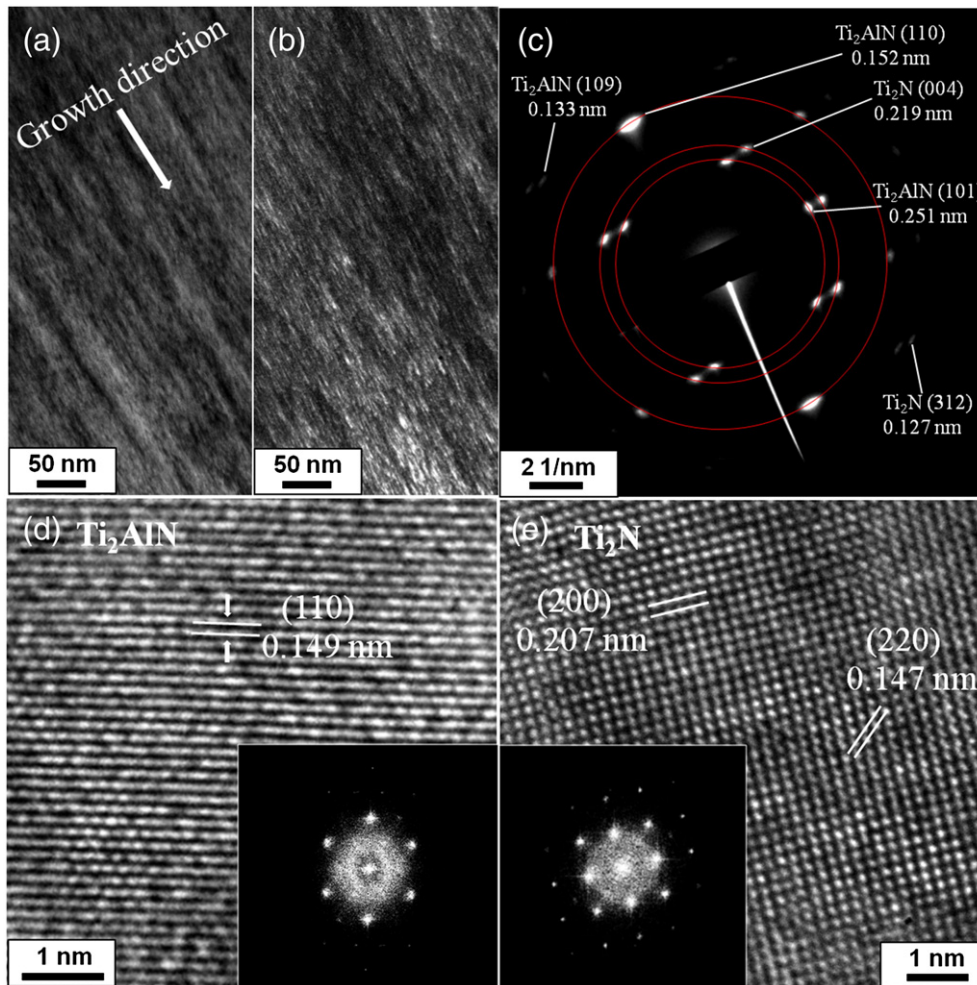


Fig. 2. 2D-XRD patterns of Ti–Al–N films deposited at 450 °C and bias voltage of –60 V.



**Fig. 3.** Cross-sectional TEM micrograph of the specimen deposited on Si(100) at 450 °C and bias voltage of  $-60$  V, (a) bright-field image from the central region of the  $\text{Ti}_2\text{AlN-Ti}_2\text{N}$  film, (b) dark-field image, and (c) selected area diffraction pattern (SADP) micrograph. HRTEM micrograph of (a)  $\text{Ti}_2\text{AlN}$  planes and (b)  $\text{Ti}_2\text{N}$  planes confirmed by d-spacing calculation and their corresponding FFT patterns (inset).

process, which exhibited phase stability of  $\text{Ti}_2\text{AlN-Ti}_2\text{N}$  films during vacuum annealing at 800 °C. According to the EPMA analysis, small amount of oxygen was incorporated into the Ti–Al–N films during film deposition from the oxygen contamination of target fabrication process and deposition process. The oxygen in the films should also contribute to the formation of  $\text{Ti}_2\text{AlN}$  MAX-phase by substituting the

N atoms in the lattices. Persson et al. [20] synthesized the MAX-phase  $\text{Ti}_2\text{Al(O,N)}$  films by a solid-state reaction between sub-stoichiometric TiN thin films and  $\text{Al}_2\text{O}_3$  (0001) substrates. The atomic ratio Ti:Al:(N+O) in our films is (0.52–0.55):(0.24–0.28):(0.18–0.21), approaching that in the  $\text{Ti}_2\text{Al(O,N)}$ , Ti:Al:(N+O) = 2:1:1.

The MAX phases are known to be synthesized usually at high temperatures. Thus, deposition temperature is the most important factor to fabricate MAX-phase films. The crystalline  $\text{Ti}_2\text{AlN}$  MAX-phase films were generally formed at high deposition temperature over 690 °C [5,27]. Much lower deposition temperature of 450 °C was, however, enough to synthesize it in this study. The reason can be attributed to the high ionization rate of metal species with relatively high ion energies, which are characteristics of HIPIMS plasma [4–9,28,29]. The increased ionization and ion energy of metal sources in the HIPIMS plasma increased the reactivity of depositing species and favored the formation of high-temperature phases. The increased ion energy of metal sources in HIPIMS plasma is believed to major contribute to crystalline  $\text{Ti}_2\text{AlN}$  MAX phase formation in our films at low temperature. On the other hand, the ion energies produced by the modulated pulse power used in this study are not so high to induce defects in the films, which was also in favor of the growth of the complicated-structured  $\text{Ti}_2\text{AlN}$  MAX phase. The low-temperature deposition of the crystalline MAX-phase  $\text{Ti}_2\text{AlN}$  films is favorable for their applications on metal/alloy substrates for industrial applications.

The formation of  $\text{Ti}_2\text{N}$  phase in the films should be attributed to the Al deficiency. Fig. 5(a) shows the crystal structure of  $\text{Ti}_2\text{AlN}$

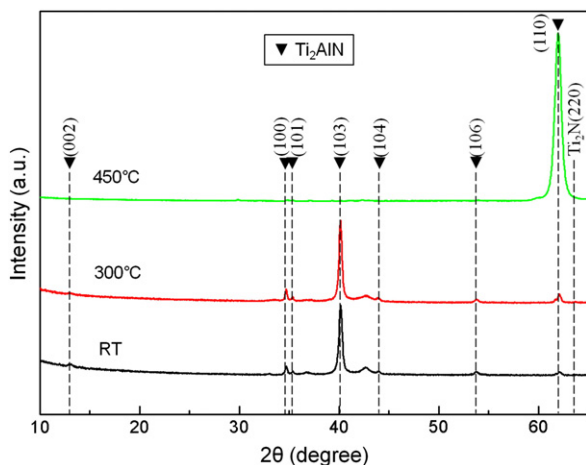


**Fig. 4.** XRD patterns of post-annealed Ti–Al–N films at 800 °C for 1 h which were deposited on Si at RT, 300 °C and 450 °C and bias voltage of  $-50$  V, respectively.

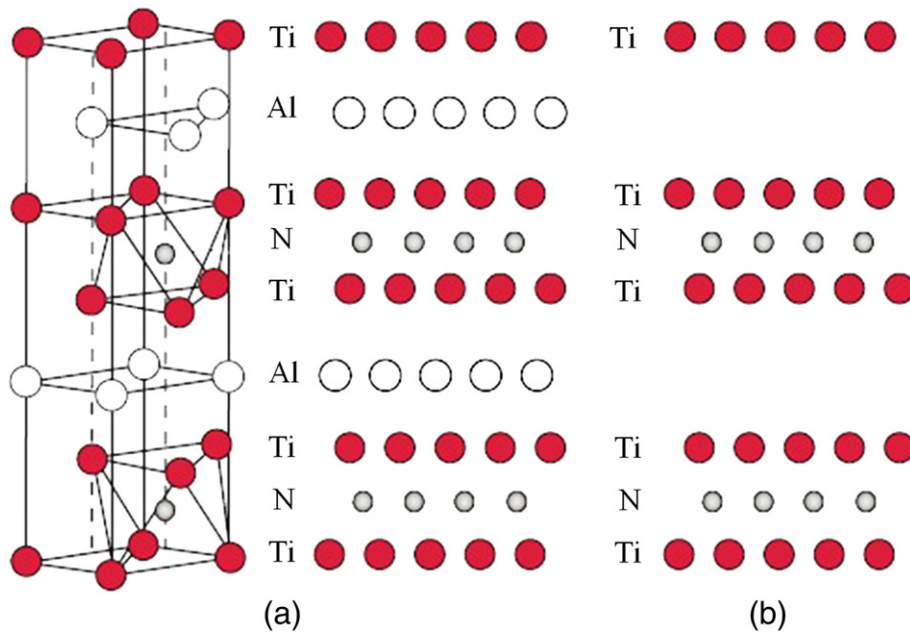


Fig. 5. The crystal structure of (a) hexagonal  $Ti_2AlN$  and (b)  $Ti_2N$ , where Al was deficient in  $Ti_2AlN$  lattice. Adapted from M. Magnuson et al. [30].

lattice, where Al atoms were interleaved in  $Ti_2N$  layers. Due to Al deficiency in the  $Ti_2AlN$  films deposited at 450 °C,  $Ti_2N$  lattice appeared, as shown in Fig. 5(b).

### 3.2. Film performance

#### 3.2.1. Mechanical properties

Fig. 6 shows the microhardness (H), elastic modulus (E), and residual stress ( $\sigma$ ) of the  $Ti_2AlN-Ti_2N$  films deposited at 450 °C as a function of applied bias voltage. The measured microhardness and elastic modulus is 13 and 178 GPa at bias voltage of 0 V, respectively. With application of negative bias voltage, the microhardness and elastic modulus values increased fastly to 19–22 GPa and 220–236 GPa, respectively. The residual stress changed from tensile stress at 0 V to compressive stress at negative bias voltages. With increasing the bias voltage, the compressive stress increased with the same tendency to those of the microhardness and elastic modulus of the films. The increase of compressive stress also resulted in the (110) peak shifting left in the XRD spectra in Fig. 1(b). The microhardness (H) of the  $Ti_2AlN-Ti_2N$  films varied from 13 to 22 GPa which is comparable to that of the TiN films while the elastic modulus (E) is in the range of 178–236 GPa, much less than that of the TiN films [31–33]. Higher H/E and  $H^3/E^2$

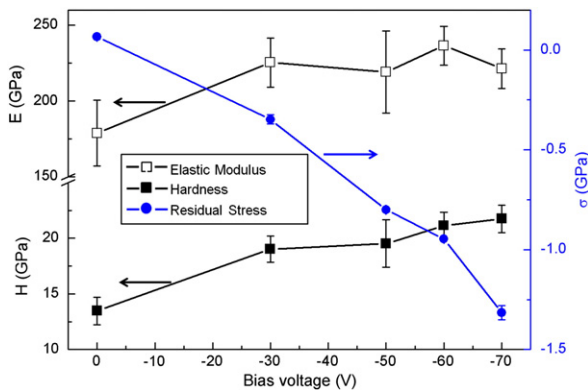


Fig. 6. Residual stress, micro-hardness and elastic modulus of the  $Ti_2AlN-Ti_2N$  thin films deposited at 450 °C as a function of bias voltage.

values mean larger elastic strain to failure and higher fracture toughness [34]. Therefore,  $Ti_2AlN-Ti_2N$  films in this study are very promising for tribological and erosion applications, much better than the TiN films. The lower elastic modulus as compared to other reported data (270–286 GPa) [3,35,36] may be due to having not enough Ti–N bonds (N-deficient) or mixing with Ti–O bonds (O-inclusion) in the films.

#### 3.2.2. Oxidation behavior

Excellent oxidation resistance is one of the characteristics of  $Ti_2AlN$  MAX phase [16]. The oxidation behavior of the  $Ti_2AlN-Ti_2N$  films composing of  $Ti_2AlN$  MAX phase and  $Ti_2N$  phase synthesized were examined in this work. As a comparison, the oxidation experiment of a (Ti,Al)N film having same Ti/Al ratio (Ti:Al  $\approx$  2:1) and stoichiometric N content ( $\sim$ 50 at.%) was also conducted. Fig. 7 shows the XRD patterns of the isothermal oxidation results of  $Ti_2AlN-Ti_2N$  and (Ti,Al)N films, respectively.

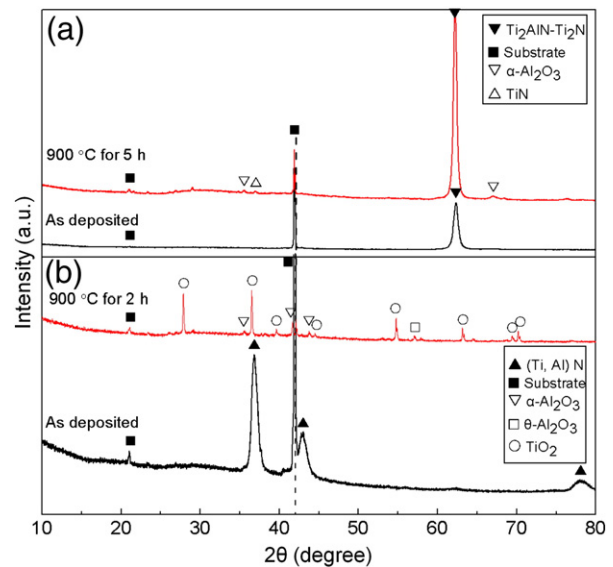


Fig. 7. XRD patterns of the isothermal oxidation results of  $Ti_2AlN-Ti_2N$  and (Ti,Al)N films, respectively.

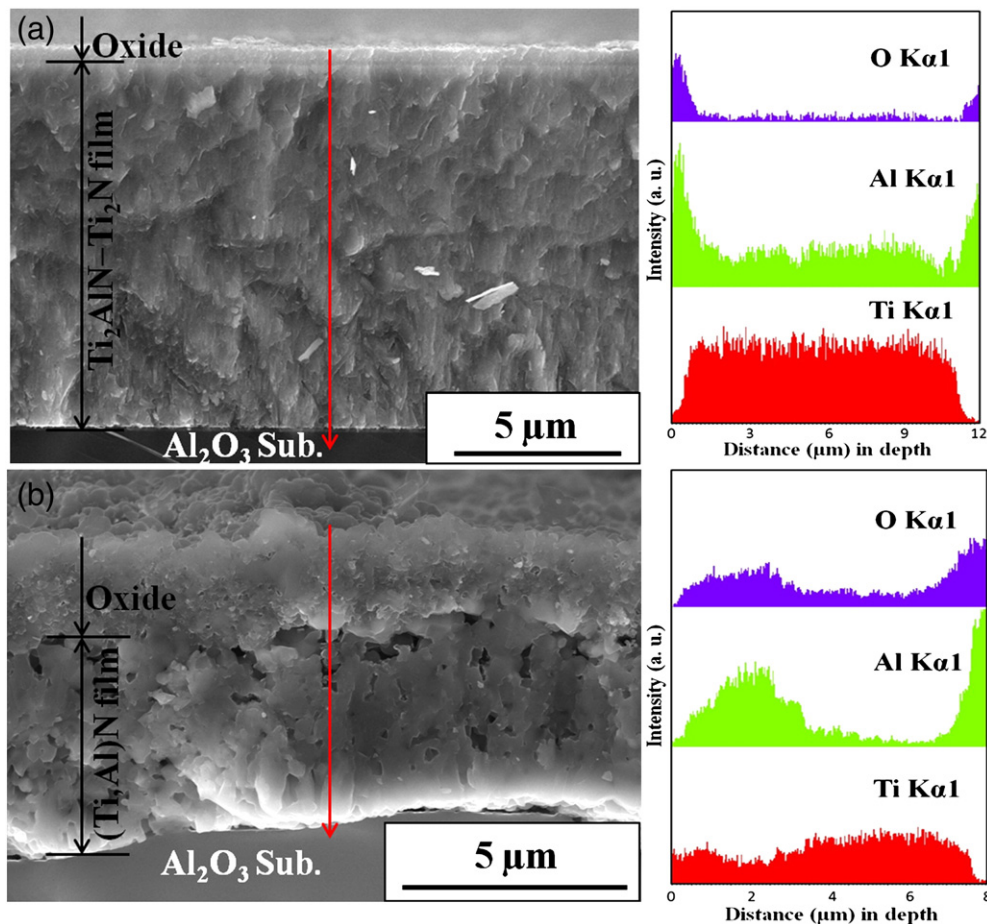


Fig. 8. Cross-sectional SEM image and the corresponding EDX line-scanning profiles of the films after isothermal oxidation, (a)  $\text{Ti}_2\text{AlN-Ti}_2\text{N}$  film at  $900^\circ\text{C}$  for 5 h, and (b)  $(\text{Ti,Al})\text{N}$  film at  $900^\circ\text{C}$  for 2 h.

$(\text{Ti,Al})\text{N}$  films, respectively. In Fig. 7(a), the (110) preferred orientation of  $\text{Ti}_2\text{AlN}$  MAX-phase remained as the main phase in the  $\text{Ti}_2\text{AlN-Ti}_2\text{N}$  films oxidized at  $900^\circ\text{C}$  for 5 h. Only weak peaks of  $\alpha\text{-Al}_2\text{O}_3$  and TiN were detected, indicating the very limited oxidation on the films. Fig. 7(b) shows that relatively strong peaks of  $\text{TiO}_2$ ,  $\alpha\text{-Al}_2\text{O}_3$  and  $\theta\text{-Al}_2\text{O}_3$  were detected instead of nitride peaks in the  $(\text{Ti,Al})\text{N}$  film

after oxidation at  $900^\circ\text{C}$  for 2 h, which indicated the severe oxidation on the  $(\text{Ti,Al})\text{N}$  film.

Fig. 8 shows fractured cross-sectional SEM images and the corresponding EDX line-scanning profiles of  $\text{Ti}_2\text{AlN-Ti}_2\text{N}$  film after oxidation at  $900^\circ\text{C}$  for 5 h, and fcc-structured  $(\text{Ti,Al})\text{N}$  film after oxidation at  $900^\circ\text{C}$  for 2 h, respectively. A continuous and homogenous  $\text{Al}_2\text{O}_3$  scale with a thickness of  $\sim 0.7\ \mu\text{m}$  was formed on the  $\text{Ti}_2\text{AlN-Ti}_2\text{N}$  film, while thick scale of Al-Ti-O mixed oxide with thickness of  $\sim 1.9\ \mu\text{m}$  was formed on the  $(\text{Ti,Al})\text{N}$  film. In addition, very low oxygen signals were observed in the remained  $\text{Ti}_2\text{AlN-Ti}_2\text{N}$  films, while significant oxygen content was detected in the  $(\text{Ti,Al})\text{N}$  film.

Due to the nanolaminated structure of  $\text{Ti}_2\text{AlN}$  MAX phase [37] where metallic Al layers positioned between covalent Ti-N layers with strong Ti-N bondings, the Al atoms are much more active and have higher diffusivity than the Ti atoms. Therefore, Al atoms in the  $\text{Ti}_2\text{AlN}$  MAX-phase diffuse out to the film surface to form a pure  $\text{Al}_2\text{O}_3$  oxide layer on the  $\text{Ti}_2\text{AlN-Ti}_2\text{N}$  film surface as soon as the oxidation starts, and the formed pure  $\text{Al}_2\text{O}_3$  oxide layer prohibits the ingress of oxygen into the films. As for the  $(\text{Ti,Al})\text{N}$  films, both Ti and Al atoms are strongly bonded to N atoms. The diffusivity of Al atoms is largely reduced as compared to the case of  $\text{Ti}_2\text{AlN}$  MAX-phase.

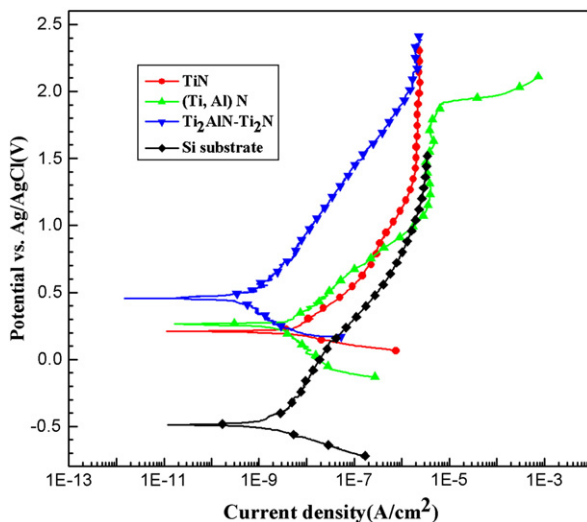


Fig. 9. The potentiodynamic polarization curves of TiN,  $\text{TiAlN}$  and  $\text{Ti}_2\text{AlN-Ti}_2\text{N}$  films, as well as Si substrate, in 3.5 wt.% NaCl aqueous solution.

Table 3

Corrosion results by potentiodynamic polarization curves obtained in 3.5 wt.% NaCl solution.

	Si	TiN	$(\text{Ti,Al})\text{N}$	$\text{Ti}_2\text{AlN-Ti}_2\text{N}$
$I_{\text{Corr}}$ ( $\text{A}/\text{cm}^2$ )	$2.54 \times 10^{-9}$	$5.79 \times 10^{-9}$	$2.76 \times 10^{-9}$	$7.93 \times 10^{-10}$
$E_{\text{Corr}}$ (V vs. Ag/AgCl)	-0.488	0.211	0.266	0.458

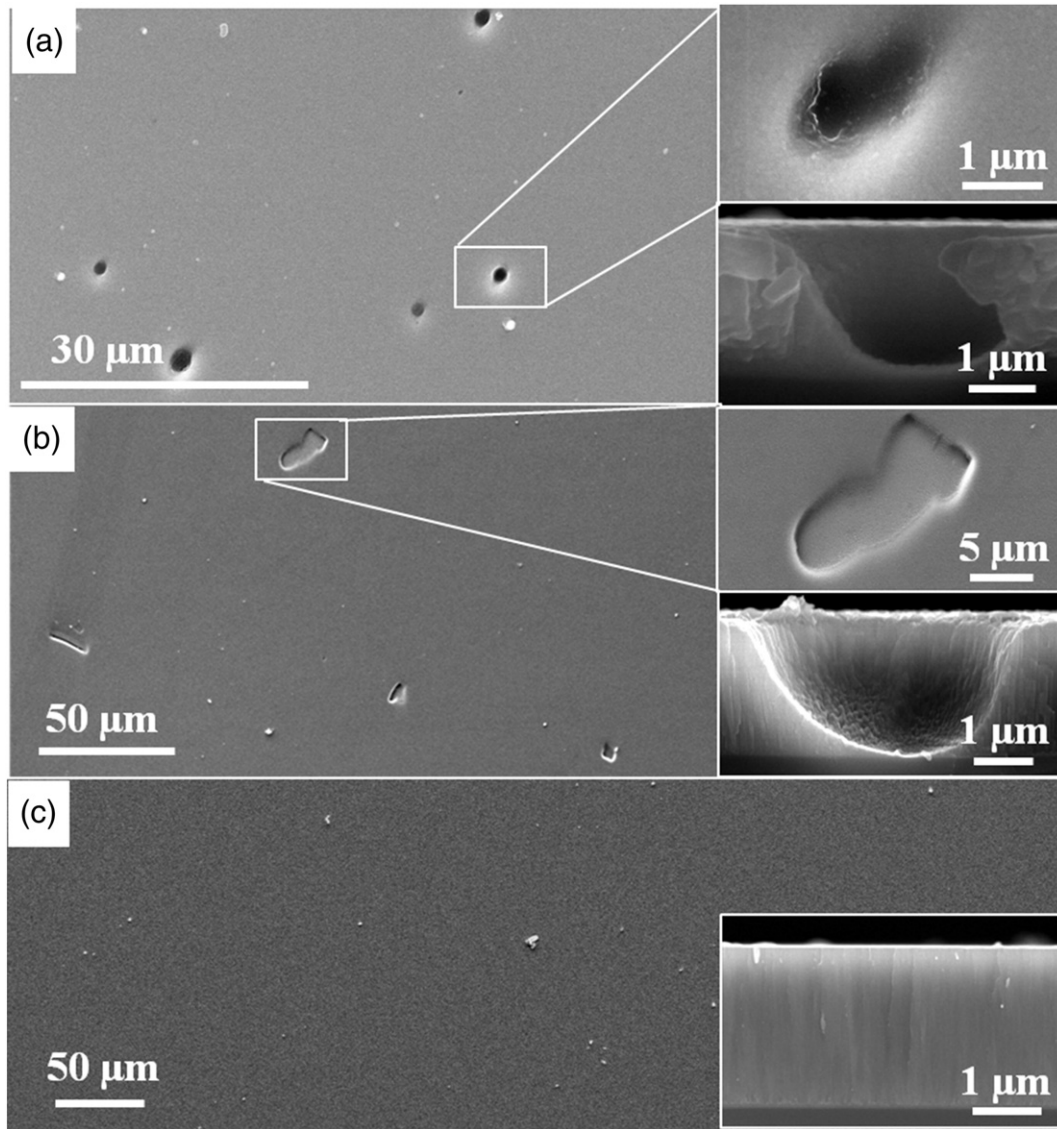


Fig. 10. Surface and cross-sectional SEM images of (a) TiN, (b) TiAlN and (c)  $\text{Ti}_2\text{AlN-Ti}_2\text{N}$  films, respectively, after corrosion testing in 3.5% NaCl aqueous solution.

Because the  $\text{Al}_2\text{O}_3$  formation is retarded due to the above-mentioned reason, the inward migration of oxygen into the (Ti,Al)N films continues without effective barriers. This phenomenon resulted in the formation of mixed oxide scale of Al-Ti-O. The mixed oxide scale of Al-Ti-O is relatively porous, and cannot play a perfect role as a diffusion barrier against further oxidation as compared with pure  $\text{Al}_2\text{O}_3$  oxide layer. Another important reason for excellent oxidation behavior of  $\text{Ti}_2\text{AlN-Ti}_2\text{N}$  films is the dense microstructure of the films. HIPIMS possesses high plasma intensity, high ionization and high average ion energy of the sputtered species, as compared to the DC pulse sputtering technique. The  $\text{Ti}_2\text{AlN-Ti}_2\text{N}$  films deposited by HIPIMS were much denser and less porous than (Ti,Al)N films synthesized using a hybrid coating system with HIPIMS and DC pulse magnetron sputtering, which made  $\text{Ti}_2\text{AlN-Ti}_2\text{N}$  films better oxidation resistance.

### 3.2.3. Corrosion behavior

The potentiodynamic polarization tests were conducted to investigate the corrosion behavior of  $\text{Ti}_2\text{AlN-Ti}_2\text{N}$ , (Ti,Al)N and TiN films. Fig. 9 shows the polarization curves of the Si specimens without and with various films. Table 3 lists the respective corrosion current densities ( $i_{\text{corr}}$ ) and the corrosion potentials ( $E_{\text{corr}}$ ). Corrosion

current was calculated using Tafel equation [38]. The corrosion current density decreased and the corrosion potential increased by applying films, which means the film layers protect the substrate from corrosive media. As compared with the TiN and (Ti,Al)N coated Si specimens, the  $\text{Ti}_2\text{AlN-Ti}_2\text{N}$  coated specimen exhibits lower corrosion current density of  $7.93 \times 10^{-10} \text{ A/cm}^2$  and higher corrosion potential of 0.458 V, indicating better corrosion resistance. Fig. 10 shows the surface and cross-sectional SEM images of TiN, (Ti,Al)N and  $\text{Ti}_2\text{AlN-Ti}_2\text{N}$  films after corrosion test. Obvious corrosive failure occurred on the TiN and (Ti,Al)N films, with fully open corrosion pits throughout the film thickness as a result of the localized corrosion attack being observed. However, in cases of the  $\text{Ti}_2\text{AlN-Ti}_2\text{N}$  film, the pitting behavior was not observed under the same experimental condition.

The  $\text{Ti}_2\text{AlN-Ti}_2\text{N}$  film performed much better corrosion resistance in the potentiodynamic polarization tests as compared to the TiN and the (Ti,Al)N films. This is due to the unique structure of  $\text{Ti}_2\text{AlN}$  MAX phase in  $\text{Ti}_2\text{AlN-Ti}_2\text{N}$  film. Due to the much higher Al activity in the  $\text{Ti}_2\text{AlN}$  MAX phase than that in the (Ti,Al)N phase, active Al atoms in the  $\text{Ti}_2\text{AlN}$  MAX phase easily diffuse out to the film surface to form a dense  $\text{Al}_2\text{O}_3$  oxide layer during the chemical attack, which passivates the surface and prevents further corrosion attack. In addition,

the Ti<sub>2</sub>AlN–Ti<sub>2</sub>N films are very dense in this study, with no pores from which the corrosive medium passing through. This could also provide good protection on the substrate.

#### 4. Conclusion

In conclusion, Ti–Al–N thin films were synthesized utilizing a high power impulse magnetron sputtering (HIPIMS) from a Ti<sub>2</sub>AlN compound target. Amorphous films formed at low deposition temperatures of RT and 300 °C, which changed into MAX-phase Ti<sub>2</sub>AlN films after vacuum annealing at 800 °C for 1 h. Films composed of MAX-phase Ti<sub>2</sub>AlN and tetragonal Ti<sub>2</sub>N phases were acquired at temperature of 450 °C, which exhibited stable film structure even vacuum annealed at 800 °C. The Ti<sub>2</sub>AlN–Ti<sub>2</sub>N films were composed of densely packed nanocrystalline fibrous grains. The microhardness and elastic modulus of the films is in the range of 19–22 GPa and 220–236 GPa, respectively. The higher H/E and H<sup>3</sup>/E<sup>2</sup> values are favorable for the tribological applications of the films. The Ti<sub>2</sub>AlN–Ti<sub>2</sub>N films exhibited excellent oxidation and corrosion resistance. The mechanism was explained with a fast formation of pure dense Al<sub>2</sub>O<sub>3</sub> layer on the top of the films due to fast out-diffusion of Al atoms, which is derived from a characteristic microstructure of MAX phase, and dense micro structure of the films, which is the merit of HIPIMS technique.

#### Acknowledgment

This work was supported by a grant from the National Core Research Center (NCRC) Program (2011-0006-256) funded by NRF and MEST. Qimin Wang acknowledges financial support from Guangzhou Scientific and Technological Planning Project (2011J2200036). Peiling Ke acknowledges financial support from International Cooperation Foundation of Ningbo Government (Grant no: 2010D10015).

#### References

- [1] M.W. Barsoum, *Solid State Chem.* 28 (2000) 201.
- [2] P.O.Å. Persson, S. Kodambaka, I. Petrov, L. Hultman, *Acta Mater.* 55 (2007) 4401.
- [3] T. Joelsson, A. Hörling, J. Birch, L. Hultman, *Appl. Phys. Lett.* 86 (2005) 111913.
- [4] J. Bohlmark, M. Lattemann, J.T. Gudmundsson, A.P. Ehiasarian, Y. Aranda Gonzalvo, N. Brenning, U. Helmersson, *Thin Solid Films* 515 (2006) 1522.
- [5] A. Hecimovic, K. Burcalova, A.P. Ehiasarian, *J. Phys. D Appl. Phys.* 41 (2008) 095203.
- [6] J. Alami, S. Bolz, K. Sarakinos, *J. Alloys Compd.* 483 (2009) 530.
- [7] J. Lin, J.J. Moore, W.D. Sproul, B. Mishra, J.A. Rees, Z. Wu, R. Chistyakov, B. Abraham, *Surf. Coat. Technol.* 203 (2009) 3676.
- [8] K. Sarakinos, J. Alami, S. Konstantinidis, *Surf. Coat. Technol.* 204 (2010) 1661.
- [9] J.L. Lin, W.D. Sproul, J.J. Moore, S. Lee, S. Myers, *Surf. Coat. Technol.* 205 (2011) 3226.
- [10] J. Alami, P. Eklund, J. Emmerlich, O. Wilhelmsson, U. Jansson, H. Högberg, L. Hultman, U. Helmersson, *Thin Solid Films* 515 (2006) 1731.
- [11] M. Beckers, N. Schell, R.M.S. Martins, A. Mücklich, W. Möller, *Appl. Phys. Lett.* 89 (2006) 074101.
- [12] M. Beckers, N. Schell, R.M.S. Martins, A. Mücklich, W. Möller, L. Hultman, *J. Appl. Phys.* 99 (2006) 034902.
- [13] T. Joelsson, A. Flück, J. Birch, L. Hultman, *J. Appl. Phys.* 102 (2007) 074918.
- [14] V. Dolique, M. Jaouen, T. Cabioch, F. Pailloux, Ph. Guérin, V. Pélousin, *J. Appl. Phys.* 103 (2008) 083527.
- [15] M. Bugnet, T. Cabioch, V. Mauchamp, Ph. Guérin, M. Marteau, M. Jaouen, *J. Mater. Sci.* 45 (20) (2010) 5547.
- [16] C. Höglund, M. Beckers, N. Schell, J.V. Borany, J. Birch, L. Hultman, *Appl. Phys. Lett.* 90 (2007) 174106.
- [17] Q.M. Wang, W. Garkas, A. Flores Renteriz, C. Leyens, K.H. Kim, *J. Nanosci. Nanotechnol.* 11 (2011) 8959.
- [18] R. Grieseler, T. Kups, M. Wilke, M. Hopfeld, P. Schaaf, *Mater. Lett.* 82 (2012) 74.
- [19] G.G. Stoney, *Proc. R. Soc. Lond., Ser. A* 82 (1909) 172.
- [20] P.O.Å. Persson, C. Höglund, J. Birch, L. Hultman, *Thin Solid Films* 519 (2011) 2421.
- [21] J. Frodelius, P. Eklund, M. Beckers, P.O.Å. Persson, H. Högberg, L. Hultman, *Thin Solid Films* 518 (2010) 1621.
- [22] H. Högberg, J. Emmerlich, P. Eklund, O. Wilhelmsson, J.-P. Palmquist, U. Jansson, L. Hultman, *Adv. Sci. Technol.* 45 (2006) 2648.
- [23] P. Eklund, M. Beckers, J. Frodelius, H. Högberg, L. Hultman, *J. Vac. Sci. Technol. A* 25 (2007) 1381.
- [24] O. Wilhelmsson, P. Eklund, H. Högberg, L. Hultman, U. Jansson, *Acta Mater.* 56 (2008) 2563.
- [25] C. Walter, D.P. Sigumonrong, T. El-Raghy, J.M. Schneider, *Thin Solid Films* 515 (2006) 389.
- [26] A. Abdulkadhim, M. to Baben, T. Takahashi, V. Schnabel, M. Hans, C. Polzer, P. Polcik, J.M. Schneider, *Surf. Coat. Technol.* 206 (2011) 599.
- [27] M. Beckers, N. Schnell, R.M.S. Martins, A. Mücklich, W. Möller, L. Hultman, *J. Appl. Phys.* 102 (2007) 074916.
- [28] J.L. Lin, J.J. Moore, W.D. Sproul, B. Mishra, Z.L. Wu, J. Wang, *Surf. Coat. Technol.* 204 (2010) 2230.
- [29] J. Paulitsch, M. Schenkel, A. Schintlmeister, H. Hutter, P.H. Mayrhofer, *Thin Solid Films* 518 (2010) 5553.
- [30] M. Magnuson, M. Mattesini, S. Li, C. Höglund, M. Beckers, L. Hultman, O. Eriksson, *Phys. Rev. B* 76 (2007) 195127.
- [31] E. Török, A.J. Perry, L. Chollet, W.D. Sproul, *Thin Solid Films* 153 (1987) 37.
- [32] G. Abadias, *Surf. Coat. Technol.* 202 (2008) 2223.
- [33] D.S. Stone, K.B. Yoder, W.D. Sproul, *J. Vac. Sci. Technol. A* 9 (1991) 2543.
- [34] A. Leyland, A. Matthews, *Wear* 246 (2000) 1.
- [35] B. Manoun, F.X. Zhang, S.K. Saxena, T. El-Raghy, M.W. Barsoum, *J. Phys. Chem. Solids* 67 (2006) 2091.
- [36] Z.J. Lin, M.J. Zhuo, M.S. Li, J.Y. Wang, Y.C. Zhou, *Scr. Mater.* 56 (2007) 1115.
- [37] Y. Zhou, Z. Sun, *Phys. Rev. B* 61 (2000) 12570.
- [38] G. Rocchini, *Corros. Sci.* 37 (6) (1995) 987.